Title

Individual Ion Binding Sites in the K+ Channel Play Distinct Roles in C-type Inactivation and in Recovery from Inactivation

Journal

Structure, 24(5)

ISSN

1359-0278

Authors

Matulef, Kimberly

Annen, Alvin W

Nix, Jay C

et al.

Publication Date

2016-05-01

DOI

10.1016/j.str.2016.02.021

Peer reviewed

Article

Structure

Individual Ion Binding Sites in the K^+ Channel Play Distinct Roles in C-type Inactivation and in Recovery from Inactivation

Graphical Abstract

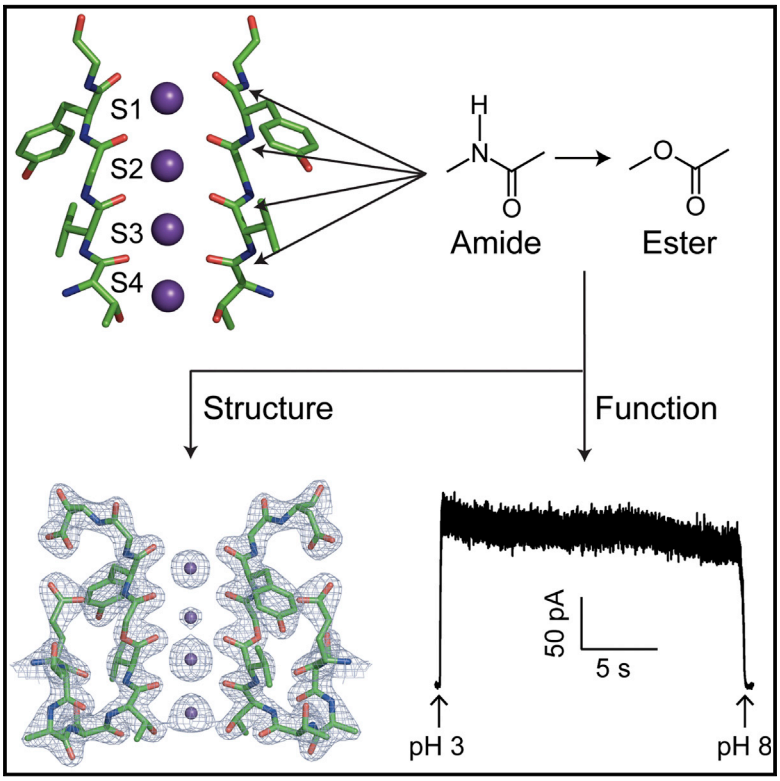

Authors

Kimberly Matulef, Alvin W. Annen, Jay C. Nix, Francis I. Valiyaveetil

Correspondence

valiyave@ohsu.edu

In Brief

C-type inactivation in K^+ channels results from a conformational change at the ion binding sites. Matulef et al. combine unnatural amide-to-ester substitutions of the protein backbone with structural and functional studies to reveal the specific roles of the individual ion binding sites during inactivation and recovery.

Highlights

- Protein backbone mutagenesis used to modify the ion binding sites in a K^+ channel
- Structures of K^+ channels with amide-to-ester substitutions in the selectivity filter
- Specific roles of the individual ion binding sites in C-type inactivation determined
- A working model for changes at the selectivity filter during C-type inactivation

Accession Numbers

5EC1
5EC2
5EBW
5EBL
5EBM

Matulef et al., 2016, Structure *24*, 750–761
May 3, 2016
http://dx.doi.org/10.1016/j.str.2016.02.021

CellPress

CellPress

Structure
Article

Individual Ion Binding Sites in the K^+ Channel Play Distinct Roles in C-type Inactivation and in Recovery from Inactivation

Kimberly Matulef,[1] Alvin W. Annen,[1] Jay C. Nix,[2] and Francis I. Valiyaveetil[1,*]
[1]Program in Chemical Biology, Department of Physiology and Pharmacology, Oregon Health & Science University, 3181 Southwest Sam Jackson Park Road, Portland, OR 97239, USA
[2]Molecular Biology Consortium, Lawrence Berkeley National Laboratory, Berkeley, CA 94720, USA
*Correspondence: valiyave@ohsu.edu
http://dx.doi.org/10.1016/j.str.2016.02.021

SUMMARY

The selectivity filter of K^+ channels contains four ion binding sites (S1–S4) and serves dual functions of discriminating K^+ from Na^+ and acting as a gate during C-type inactivation. C-type inactivation is modulated by ion binding to the selectivity filter sites, but the underlying mechanism is not known. Here we evaluate how the ion binding sites in the selectivity filter of the KcsA channel participate in C-type inactivation and in recovery from inactivation. We use unnatural amide-to-ester substitutions in the protein backbone to manipulate the S1–S3 sites and a side-chain substitution to perturb the S4 site. We develop an improved semisynthetic approach for generating these amide-to-ester substitutions in the selectivity filter. Our combined electrophysiological and X-ray crystallographic analysis of the selectivity filter mutants show that the ion binding sites play specific roles during inactivation and provide insights into the structural changes at the selectivity filter during C-type inactivation.

INTRODUCTION

K^+ channels play important roles in essential cellular processes such as the maintenance of the resting membrane potential, the excitation of nerve and muscle cells, the secretion of hormones, and sensory transduction (Hille, 2001). Important for the physiological function of K^+ channels is their ability to selectively conduct K^+ (Hille, 2001). The ion conduction pathway in a K^+ channel is contained within the pore domain whose topology is conserved in the K^+ channel family (Figure 1A) (MacKinnon et al., 1998). Selection for K^+ takes place in the narrow region of the ion pathway referred to as the selectivity filter (MacKinnon, 2004). The selectivity filter consists of a row of four K^+ binding sites that are built using the main chain carbonyl oxygen atoms and the threonine side chain from the protein sequence T-V-G-Y-G (Figure 1B) (Doyle et al., 1998; Zhou et al., 2001). This sequence is highly conserved in K^+ channels, and known structures of K^+ channels show a similar structure for the selectivity filter (Jiang et al., 2003; Long et al., 2007; Tao et al., 2009).

In addition to determining K^+ selectivity, the selectivity filter acts as a gate to regulate the flow of ions (Hoshi and Armstrong, 2013; Kurata and Fedida, 2006; McCoy and Nimigean, 2012). This process of gating at the selectivity filter has been extensively investigated in voltage-gated K^+ (K_v) channels and is referred to as C-type (or slow) inactivation (Hoshi et al., 1991). During C-type inactivation, conformational changes at the selectivity filter convert it from a conductive to a non-conductive state. While there is a large body of experimental work implicating the selectivity filter in C-type inactivation, the molecular details of the conformational changes that take place at the selectivity filter to restrict the movement of ions are not known (Hoshi and Armstrong, 2013; Kurata and Fedida, 2006). The movement of ions through the pore domain is additionally controlled by the activation gate, which is formed by the bundle crossing of the transmembrane helices at the cytoplasmic side of the pore (Figure 1A) (Jiang et al., 2002; Liu et al., 1997; Perozo et al., 1999). In the closed state, the bundle crossing obstructs the movement of K^+ through the pore (Figure 1C). Channel activation causes a widening of the helix bundle to permit the flow of K^+ through the pore. The process of activation and C-type inactivation are coupled (Cuello et al., 2010a; Panyi and Deutsch, 2006). The opening of the activation gate triggers C-type inactivation at the selectivity filter while the closure of the activation gate is required for the selectivity filter to recover from the inactivated state to the conductive state. This balance of the rates of inactivation and recovery determines the number of K^+ channels available for subsequent activation and, therefore, determines the excitability of the cell (Hoshi and Armstrong, 2013).

Gating of ion conduction at the selectivity filter is also observed in channels that do not belong to the K_v family such as the bacterial K^+ channel, KcsA. KcsA is a pH-gated channel, activated by a decrease in intracellular pH that opens the gate at the bundle crossing (Cuello et al., 1998). Activation of the KcsA channel results in a rapid increase in current and is followed by inactivation, during which the current spontaneously decays to a low steady value (Figure 1D) (Chakrapani et al., 2007; Cordero-Morales et al., 2006a; Gao et al., 2005). Recovery of the channel from inactivation requires closure of the activation gate, which takes place for the KcsA channel with a change in the intracellular pH from acidic to neutral values (Figure 1D) (Chakrapani et al., 2007). This process of inactivation in the

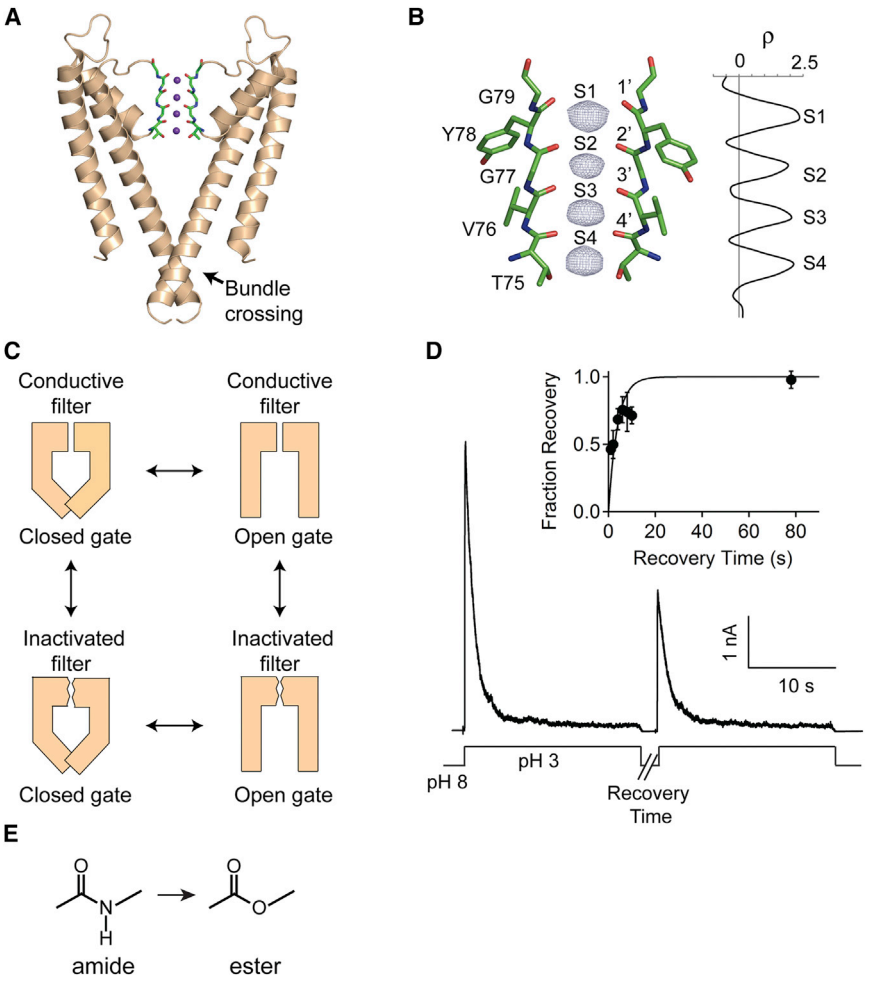

Figure 1. The Selectivity Filter and Inactivation in the KcsA Channel

(A) Structure of the wild-type KcsA channel (PDB: 1K4C). Two opposite subunits of the tetramer are shown with the selectivity filter (residues T75–G79) depicted as sticks and K^+ ions bound to the selectivity filter shown as spheres.

(B) Close-up of the selectivity filter of the KcsA channel. The amide bonds (1′–4′) and the ion binding sites (S1–S4) are labeled. The F_o-F_c electron density (residues 75–79, ions and lipid omitted) present at the ion binding sites is shown, contoured at 3.0σ. A one-dimensional plot of the electron density sampled along the central axis of the selectivity filter is shown (right).

(C) The gating cycle of the KcsA channel. Four states are depicted with the selectivity filter in either the conductive or the inactivated state and the bundle crossing in either the closed or the open state. The changes at the bundle crossing and the selectivity filter are coupled. Opening of the bundle crossing favors the inactivated state of the selectivity filter while closure of the bundle crossing favors the conductive state.

(D) Macroscopic currents for the KcsA channel were elicited at +80 mV by two pulses to pH 3.0 with a variable time interval (recovery time) at pH 8.0 between pulses. The fraction recovery was measured as the ratio of the peak current in the second pulse to the peak current in the first pulse. Inset: the fraction recovery plotted as a function of the recovery time at pH 8.0. Points represent the mean ± SD from 3–4 patches and the solid line is a fit to a single exponential function.

(E) Amide-to-ester mutagenesis.

KcsA channel is functionally similar to C-type inactivation in K_v channels (Cordero-Morales et al., 2006b, 2007, 2011; Cuello et al., 2010b). This similarity, combined with the easy amenability of KcsA to structural and spectroscopic studies, has made it an important experimental system for the investigation of the process of C-type inactivation (Ader et al., 2009; Bhate and McDermott, 2012; Cuello et al., 2010b; Imai et al., 2010).

It has been established that ion binding to the selectivity filter modulates C-type inactivation, but the underlying mechanism is not known (Kurata and Fedida, 2006). In this work, we address how the ion binding sites in the selectivity filter of the KcsA channel participate in inactivation and recovery from inactivation. Our approach is to perturb ion binding at specific sites in the filter and determine the role of each site in inactivation and recovery. The S1–S3 sites (see Figure 1B for nomenclature) in the selectivity filter are made up entirely by the carbonyl oxygens of the protein backbone, and to manipulate these sites we use amide-to-ester substitutions in the protein backbone (Figure 1E). An ester bond is isosteric to an amide bond but shows lower electronegativity at the carbonyl oxygen, by roughly one-half (Powers et al., 2005). The lower electronegativity at the liganding oxygens leads to lower ion binding at the site. As the protein backbone is not accessible to traditional site-directed mutagenesis, we use protein semisynthesis to introduce the ester substitutions into the selectivity filter. Semisynthesis is a very powerful approach for protein engineering as it allows protein modification using chemical synthesis (Muir, 2003). Semisynthesis consists of assembly of the polypeptide from recombinant and synthetic fragments using native chemical ligation (NCL), followed by in vitro folding to the native state. NCL is a coupling reaction between a C-terminal thioester peptide and an N-terminal Cys peptide that results in linking the peptides with a native peptide bond (Dawson et al., 1994). Recently, we applied this backbone mutagenesis approach to alter ion occupancy at the S1 and S2 sites to investigate their roles in inactivation (Matulef et al., 2013). We found that decreasing ion occupancy at the S1 site with the G79ester substitution did not affect the rate of inactivation, while decreasing occupancy at the S2 site with the Y78ester substitution nearly eliminated inactivation. We also found that the G77ester mutation nearly eliminated inactivation. At that time, technical limitations of the semisynthetic approach prevented us from generating sufficient yields of the G77ester channel for structural studies or from generating sufficient yields of the V76ester for functional or structural studies.

Here, we develop an improved semisynthetic approach for generating amide-to-ester substitutions in the selectivity filter. We use this modified semisynthetic approach along with traditional mutagenesis to alter ion occupancy at all the ion binding

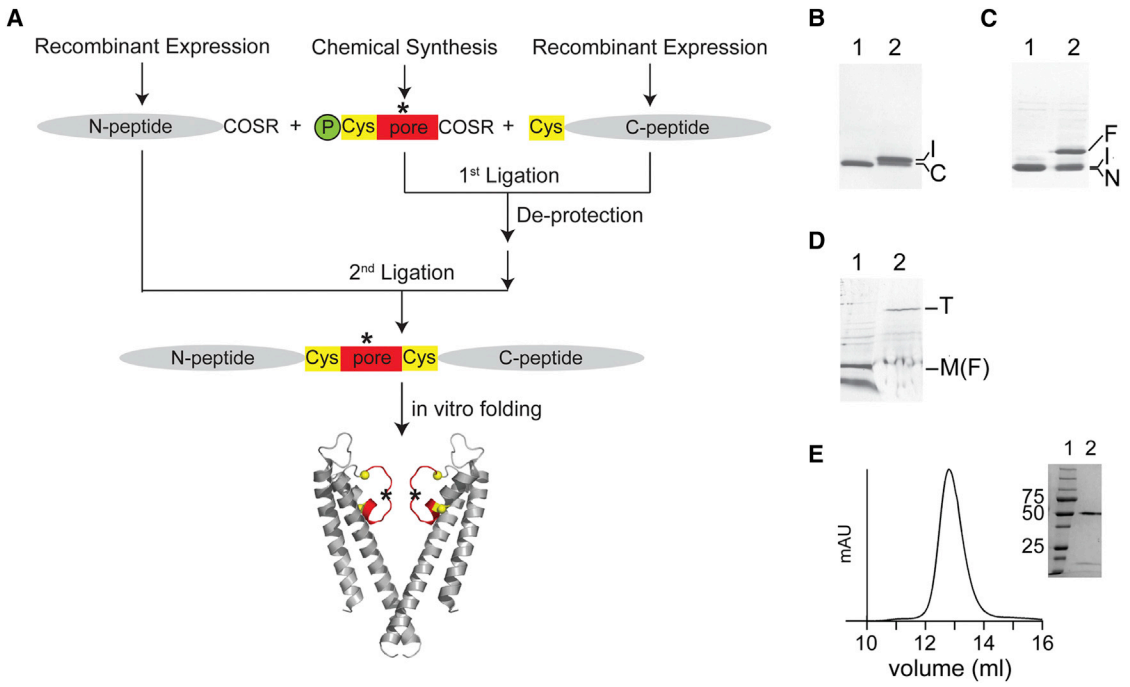

Figure 2. Modular Semisynthesis of the KcsA V76ester Channel

(A) Strategy for the semisynthesis of the KcsA V76ester channel. The KcsA polypeptide is synthesized from two recombinant peptides (gray; N-peptide thioester, residues 1–69 and C-peptide, 82–160) and a synthetic pore peptide thioester (red; residues 70–81) by two sequential native chemical ligation reactions. The V76ester linkage in the pore peptide is indicated by an asterisk. The first ligation reaction between the C-peptide and the pore peptide thioester yields an intermediate peptide. The Thz protecting group (green sphere) on the N-terminal cysteine of the intermediate peptide is removed, and the intermediate peptide is then ligated to the N-peptide thioester to yield the KcsA polypeptide. The KcsA polypeptide is folded in vitro to the native state. The ligation sites, residues 70 and 82, are represented by yellow boxes or spheres.

(B) SDS-PAGE gel (15%) of the first ligation reaction between the C-peptide (C) and the V76ester pore peptide (residues 70–81, with the peptide bond between residues 75 and 76 replaced with an ester linkage) to form the intermediate peptide (I) at 0 min (lane 1) and 2 hr (lane 2).

(C) SDS-PAGE gel (15%) of the second ligation reaction between the N-peptide thioester (N) and the intermediate peptide to form the KcsA polypeptide (F) at 0 min (lane 1) and 24 hr (lane 2).

(D) SDS-PAGE gel (12%) showing the folding of semisynthetic KcsA by lipids. The unfolded monomeric (M, which corresponds to the KcsA polypeptide) and the folded tetrameric KcsA (T) are indicated.

(E) Size-exclusion chromatography of the purified V76ester KcsA channel. Inset: SDS-PAGE gel (12%) showing molecular weight markers (lane 1) and the purified V76ester channel (lane 2).

sites in the selectivity filter. By using a combination of structural and functional approaches, we determine the roles of the selectivity filter sites in inactivation and in recovery from inactivation. The distinct roles of the ion binding sites provide insights into the structural changes at the selectivity filter that underlie C-type inactivation.

RESULTS

An Optimized Semisynthetic Approach for Introducing Ester Substitutions in the Selectivity Filter

To alter ion occupancy at the S3 site, we sought to generate the KcsA V76ester channel in which the 4′ amide bond in the selectivity filter is replaced with an ester linkage. This was a synthetically challenging endeavor, as the 4′ amide bond links two β-branched amino acids, Thr75 and Val76 (Figure 1B). Forming an ester linkage between residues with a β-branched side chain is difficult due to steric hindrance (Kent, 1988). We initially attempted semisynthesis of the V76ester channel using the previously reported two-part approach (Matulef et al., 2013; Valiyaveetil et al., 2004). For introducing the ester substitution using semisynthesis, the ester linkage is initially incorporated into a synthetic peptide, which is then used for the assembly of the KcsA channel. The two-part semisynthesis calls for the incorporation of the V76ester linkage into a 55-amino-acid-long peptide. This approach was not successful as we were not able to synthesize the V76ester peptide required in sufficient yields. Next, we explored using the three-part "modular" semisynthesis (Komarov et al., 2009). In the modular approach, the KcsA channel is assembled from three peptides: a synthetic peptide thioester (pore peptide), which encompasses the selectivity filter, and two recombinant peptides corresponding to the rest of the channel (Figure 2A). The peptides are coupled together by two sequential NCL reactions followed by in vitro folding to the native state. The key advantage of the modular approach is that the peptide into which the ester linkage has to be incorporated is relatively short, i.e., 12 amino acids compared with 55 amino acids for the two-part approach. The shorter length is advantageous in both the synthesis and purification of the ester-containing peptide.

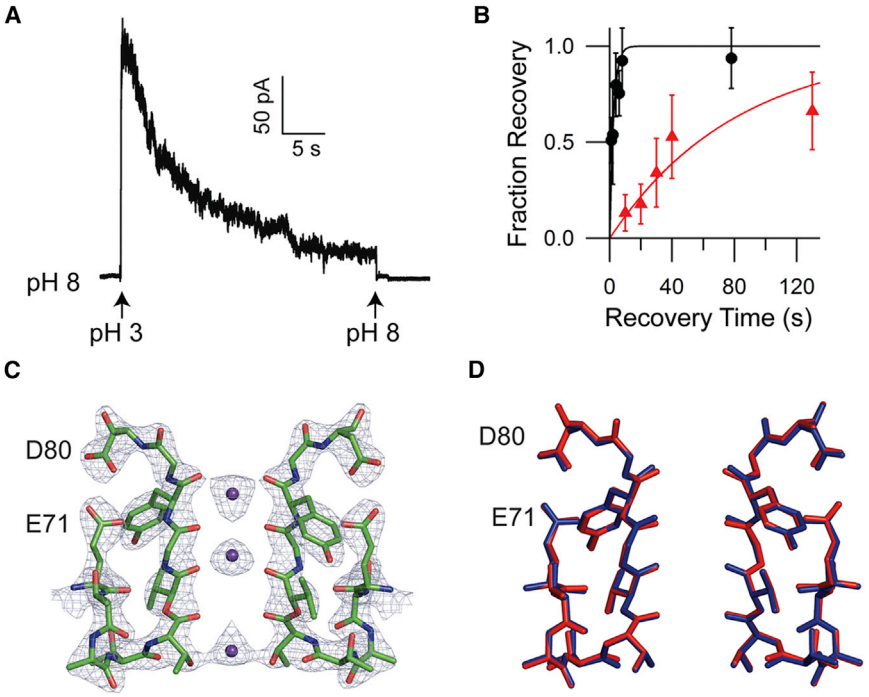

Figure 3. Functional and Structural Effects of the V76ester Substitution

(A) Macroscopic currents for the KcsA V76ester channel were elicited at +80 mV by a rapid change in pH.

(B) Recovery from inactivation in the V76ester (red triangles) and the control channel (black circles). The control channel contains the amino acid substitutions (S69A, V70C, and Y82C) that are present in the semisynthetic channels. Data points represent the mean ± SD from 3–10 patches. The solid lines are single exponential fits.

(C) Structure of the selectivity filter of the V76ester channel. The $2F_o$-F_c electron density map contoured at 2.8σ for diagonally opposite subunits is shown with residues 71–80 represented as sticks and the K^+ ions in the filter represented as spheres.

(D) Superposition of selectivity filter of the wild-type (blue) and the V76ester channel (red).

For the synthesis of the V76ester pore peptide, we initially attempted to generate the ester linkage between Thr75 and Val76 using the previously published conditions, but obtained poor yields (Matulef et al., 2013; Valiyaveetil et al., 2006b). To improve the yields, we tested alternative coupling reagents and identified COMU (1-[(1-(cyano-2-ethoxy-2-oxoethylideneaminooxy)-dimethylaminomorpholinomethylene)]-methanaminium-hexafluorophosphate) as the optimal coupling reagent for introducing the ester linkage (Twibanire and Grindley, 2011). This modification enabled synthesis of the V76ester pore peptide with good yields. We used the V76ester pore peptide to assemble the KcsA polypeptide by NCL reactions and folded it to the native tetrameric state using the lipid-based in vitro folding procedure to obtain the KcsA V76ester channels (Figures 2B–2D). The KcsA V76ester mutant channels were purified from the lipid vesicles for functional and structural studies (Figure 2E). Using our optimized modular approach, we were able to routinely generate ~0.5 mg of the purified KcsA V76ester channel. In addition to the V76ester mutant, we used this modular approach for the assembly of the G79ester and the G77ester channels in good yields.

Functional and Structural Effects of the V76ester Substitution in the Selectivity Filter

We incorporated the purified KcsA V76ester channels into lipid vesicles and used liposome patch clamping to measure channel activity. Macroscopic currents for the V76ester channel were elicited by a pH jump from 8.0 to 3.0 on the cytoplasmic side and showed rapid activation followed by inactivation (Figure 3A). The rate of inactivation of the V76ester mutant was slightly slower (~2-fold) compared with the control channel (Table 1). We used a paired pH pulse protocol to measure the recovery from inactivation and observed that recovery from inactivation was dramatically slower (~30-fold) in the V76ester mutant than in the control (Figure 3B and Table 1).

To investigate the effect of the V76ester substitution on the structure and ion occupancy in the selectivity filter, we determined the crystal structure of the V76ester channel. For structure determination, the V76ester channel was crystallized as a complex with Fab (Zhou et al., 2001). These attempts yielded crystals that diffracted to 2.9-Å resolution. The structure was determined by molecular replacement, and the electron density map corresponding to the selectivity filter of the V76ester mutant is shown (Figure 3C and Table 2). Superposition of the selectivity filters of the V76ester and the wild-type KcsA channel reveals no appreciable differences in the protein structures (Figure 3D). Unlike the wild-type KcsA channel, which shows roughly equal ion occupancy at the four ion binding sites (Figure 1B; Zhou and MacKinnon, 2003), the V76ester shows no detectable electron density at the S3 site (Figure 3C), indicating that the V76ester substitution specifically decreases ion binding to the S3 site.

Ion Occupancy at the S3 Site Is Required for Recovery from Inactivation

To verify that our conclusions on the effect of the V76ester substitution on the structure and ion occupancy were not skewed by the moderate resolution of the data, we pursued crystals that diffracted to a higher resolution. To this end, we introduced an additional G77→D-Alanine (dA) substitution, as the KcsA-G77dA channel readily crystallizes and affords crystals that diffract to a higher resolution (Valiyaveetil et al., 2006a). Furthermore, the G77dA substitution does not alter the structure or ion occupancy of the selectivity filter and, importantly, does not alter that rate of C-type inactivation or recovery from inactivation (Figures 4A, 4B, and 4D; Table 1) (Devaraneni et al., 2013; Valiyaveetil et al., 2006a).

We synthesized a pore peptide with the V76ester + G77dA substitutions and used the modular approach for assembly of the KcsA V76ester + G77dA channel. Functional measurements on the KcsA V76ester + G77dA channels showed a rate of inactivation that was similar to the wild-type control (or the G77dA

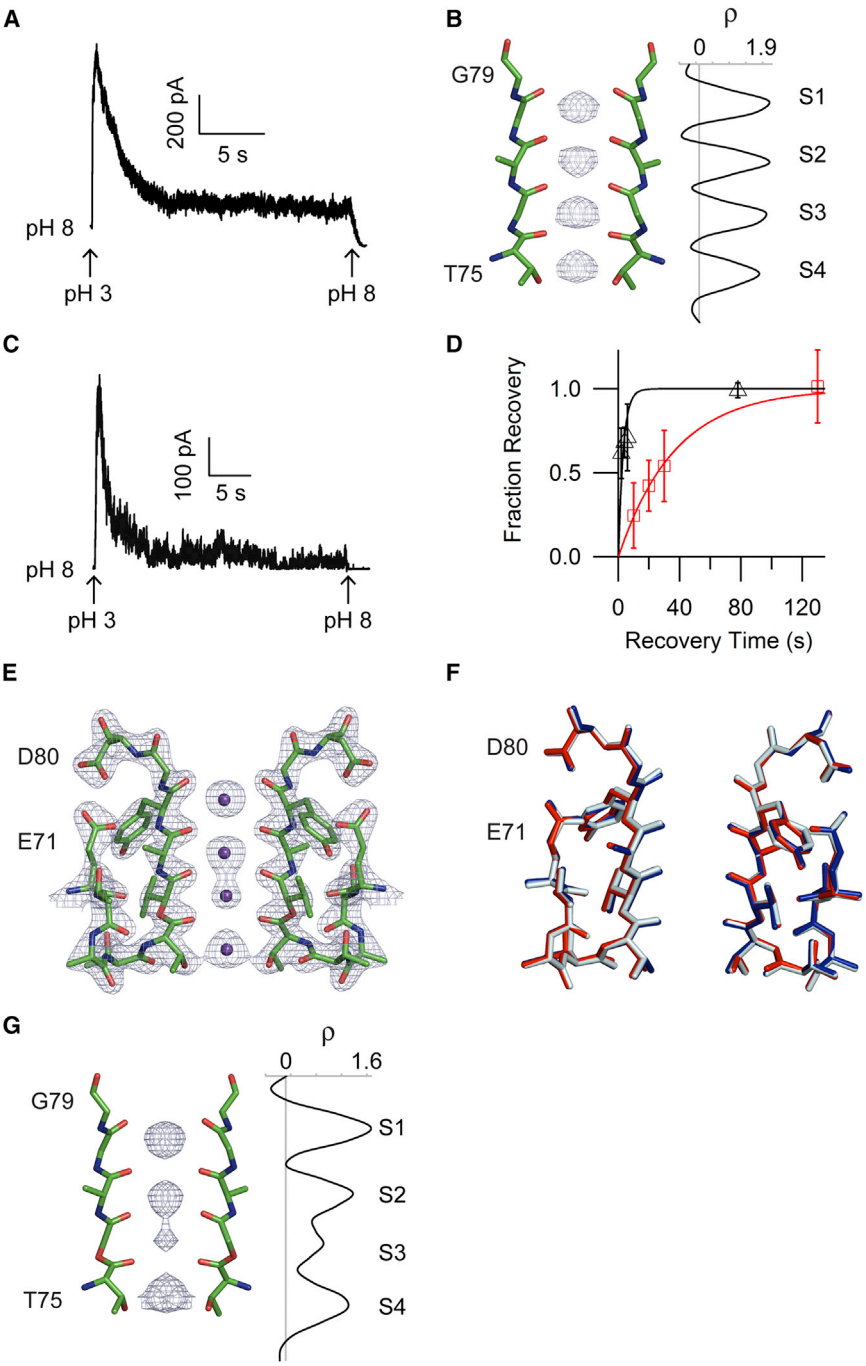

Figure 4. Incorporating the G77dA Substitution into the KcsA V76ester Channel

(A) Macroscopic currents for the KcsA G77dA channel elicited at +80 mV by a rapid change in pH.

(B) The ion binding sites in the selectivity filter of the KcsA G77dA channel (PDB: 2IH3). Two opposite subunits are shown as sticks. Side chains of V76 and Y78 are omitted for clarity. The F_o-F_c electron density (KcsA residues 75–79, K^+ ions and lipid omitted) along the central axis of the selectivity filter contoured at 3.0σ is shown. The one-dimensional plot of the electron density is shown on the right.

(C) Macroscopic currents for the KcsA V76ester + G77dA channel elicited at +80 mV by a rapid change in pH.

(D) Recovery from inactivation in the G77dA (black triangles) and the V76ester + G77dA channels (red squares). Data points represent the mean ± SD from 3–6 patches. The solid lines are single exponential fits.

(E) Structure of the selectivity filter of the V76ester + G77dA channel. The $2F_o$-F_c electron density map contoured at 2.8σ is shown with residues 71–80 of the channel represented as sticks and K^+ ions in the filter represented as spheres.

(F) Superposition of residues 71–80 of the V76ester + G77dA channel (red) with the G77dA (blue, PDB: 2IH3) and the wild-type channels (gray, PDB: 1K4C).

(G) The ion binding sites in the selectivity filter of the V76ester + G77dA KcsA channel. The F_o-F_c electron density (KcsA residues 75–79, K^+ ions and lipid omitted) contoured at 3.0σ is shown along the central axis of the selectivity filter. The one-dimensional plot of the electron density is shown on the right.

channel) while the recovery from inactivation was ~15-fold slower than the control (Figures 4C and 4D; Table 1). The inactivation properties of the KcsA V76ester + G77dA channel are therefore qualitatively similar to the V76ester channel.

As anticipated, we were able to obtain structural data to a higher resolution (2.5 Å) with the V76ester + G77dA channel (Table 2). The electron density of the selectivity filter region is shown in Figure 4E. A superposition of the selectivity filter of the V76ester + G77dA channel with the G77dA and the wild-type KcsA channels is shown in Figure 4F. The structure of the V76ester + G77dA mutant channel is basically identical to the G77dA channel. Comparison with the wild-type channel structure shows a slight rotation of the Y78 side chain, which is also observed in the G77dA structure. The electron density corresponding to K^+ ions in the selectivity filter shows a decrease in the electron density at the S3 site, indicating substantially reduced ion binding specifically at the S3 site in the mutant channel (Figure 4G). We observe a very slight shift (~0.1 Å) of the S2 and S4 ions toward the S3 site.

The major effect of the V76ester substitution is to reduce ion occupancy at the S3 site, and the functional effect is to impair recovery from inactivation. Our results therefore suggest that recovery from inactivation requires ion occupancy at the S3 site. Furthermore, we observe a similar effect on inactivation due to the V76ester substitution in the wild-type or the G77dA background. The G77dA substitution blocks the selectivity filter from attaining the constricted or the collapsed state that is observed for the KcsA channel at low K^+ concentrations or with the activation gate in the open state (Cuello et al., 2010b; Devaraneni et al., 2013; Valiyaveetil et al., 2006a; Zhou

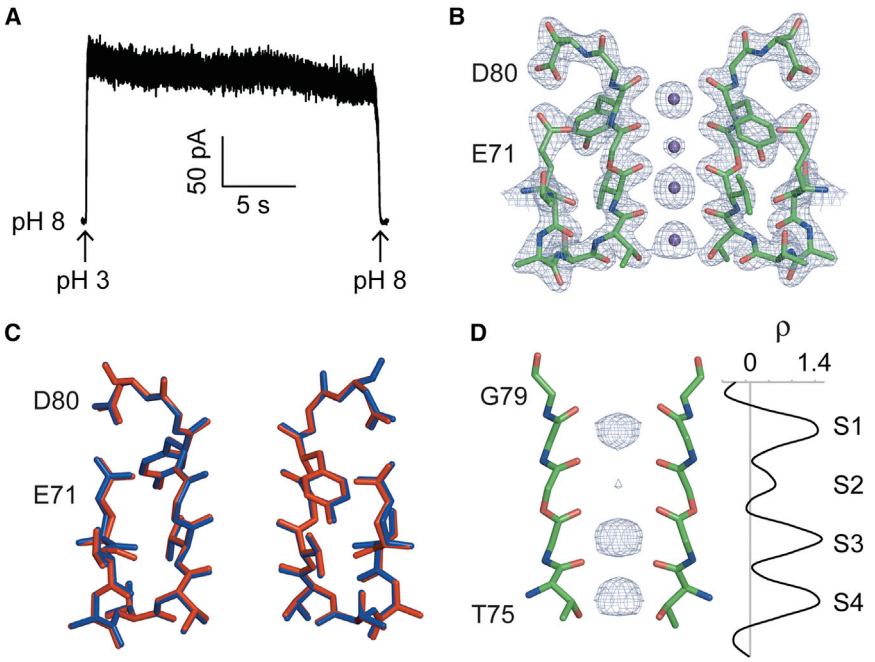

Figure 5. Effects of the G77ester Substitution on Inactivation and Ion Distribution in the Selectivity Filter

(A) Macroscopic currents elicited at +80 mV for the KcsA G77ester channels by a rapid change in pH.

(B) Structure of the selectivity filter of the KcsA G77ester channel. The $2F_o$-F_c electron density map contoured at 2.8σ is shown with residues 71–80 of the channel represented as sticks and K^+ ions in the filter represented as spheres.

(C) Superposition of residues 71–80 of the KcsA G77ester (red) and the wild-type channel (blue).

(D) The ion binding sites in the selectivity filter of the G77ester channel. The F_o-F_c electron density (KcsA residues 75–79, K^+ ions and lipid omitted) along the central axis of the selectivity filter contoured at 2.5σ is shown. The one-dimensional plot of the electron density is shown on the right.

et al., 2001). These measurements therefore also indicate that the impaired recovery observed with the V76ester substitution does not arise from the filter transitioning to the constricted state.

Ion Occupancy at the S2 Site Is Required for Inactivation

The S3 binding site is formed by the carbonyl oxygens of the 3′ and the 4′ amide bond (Figure 1B). We have previously demonstrated that the 3′ amide-to-ester substitution (G77ester) impairs the ability of the channel to undergo C-type inactivation (Matulef et al., 2013). The 3′ carbonyl oxygen contributes to both the S2 and S3 sites. To determine the effect of the 3′ ester substitution on the ion occupancies at these sites, we solved the structure of the KcsA G77ester channel. We were able to assemble the KcsA G77ester channel using either the modular approach or two-part semisynthesis. Functional measurements on the KcsA G77ester channel showed a lack of inactivation (Figure 5A), as previously reported (Matulef et al., 2013). We determined the crystal structure of the KcsA G77ester and refined it to 2.3-Å resolution. The electron density corresponding to the selectivity filter is shown in Figure 5B. A superposition of the G77ester and the wild-type channel (Figure 5C) shows that the ester substitution is well tolerated, with no noticeable structural changes in the ion binding sites or in the amino acid side chains surrounding the selectivity filter. The G77ester mutant shows altered ion occupancy in the selectivity filter, with the ester substitution nearly eliminating all ion occupancy at the S2 site while having no effect on the ion occupancies at the other sites (Figure 5D). We observe a slight shift in the positions of the S1 and S3 ions (~0.3 Å) toward the S2 site. The Y78ester substitution that has a similar phenotype of reduced C-type inactivation also shows reduced ion occupancy at the S2 site (Figure S1) (Matulef et al., 2013). The results observed with the Y78ester and the G77ester channels therefore indicate that lower ion occupancy at the S2 site impairs inactivation.

Ion Occupancy at the S1 Site Is Not Important for Inactivation or Recovery

Next, we investigated the role of ion binding at the S1 site in C-type inactivation. The S1 site has been proposed as the locus for the conformational changes that result in C-type inactivation (Armstrong and Hoshi, 2014; Hoshi and Armstrong, 2013). The G79ester substitution in the selectivity filter reduces ion occupancy at the S1 site; therefore, we used the KcsA G79ester channel to evaluate the role of the S1 site (Figure 6A) (Valiyaveetil et al., 2006b). We assembled the full-length G79ester channel

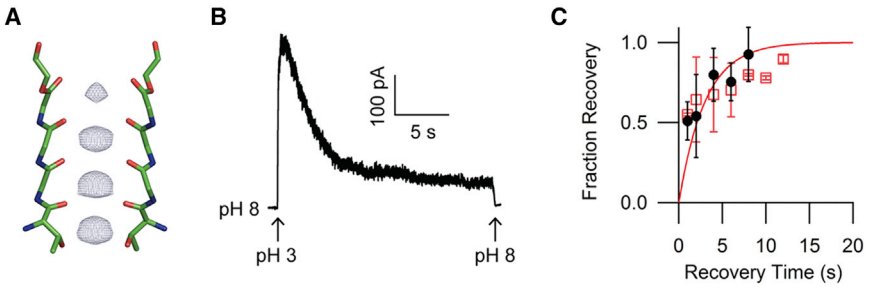

Figure 6. Inactivation and Recovery in the KcsA G79ester Channel

(A) The ion binding sites in the selectivity filter of the KcsA G79ester channel. Two opposite subunits are shown in stick representation (PDB: 2H8P). F_o-F_c electron density (KcsA residues 75–79, K^+ ions and lipid omitted) along the central axis of the selectivity filter contoured at 3.0σ is shown.

(B) Macroscopic currents for the KcsA G79ester channel elicited at +80 mV by a rapid change in pH.

(C) Recovery from inactivation of G79ester (red squares) and control channels (black circles). Data points represent the mean ± SD from 3–5 patches, and the solid line represents an exponential fit to the data for the G79ester channel.

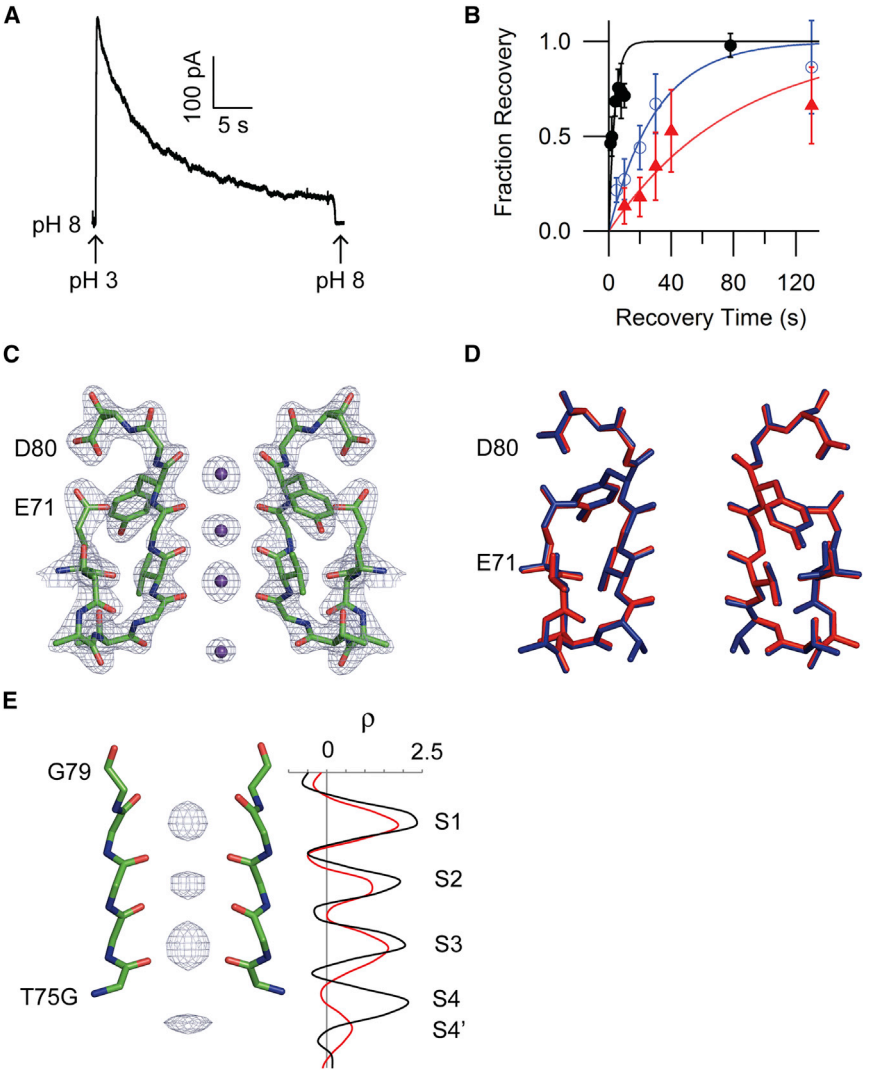

Figure 7. Effects of the T75G Substitution on Inactivation and Ion Distribution in the Selectivity Filter

(A) Macroscopic currents for the KcsA T75G channels elicited at +80 mV by a rapid change in pH.

(B) Recovery from inactivation in the KcsA T75G (blue open circles), V76ester (red triangles), and wild-type channels (black closed circles). Data points represent the mean ± SD from 3–7 patches and the solid lines are single exponential fits. Data for the V76ester and the wild-type channel are from Figures 3B and 1D, respectively.

(C) Structure of the selectivity filter of the KcsA T75G channel. The $2F_o$-F_c electron density map contoured at 2.5σ is shown with residues 71–80 of the channel represented as sticks and K^+ ions in the filter represented as spheres.

(D) Superposition of residues 71–80 of the KcsA T75G (red) and the wild-type channel (blue).

(E) The ion binding sites in the selectivity filter of the T75G channel. The F_o-F_c electron density (KcsA residues 75–79, K^+ ions, and lipid omitted) along the central axis of the selectivity filter contoured at 3.0σ is shown. The one-dimensional plot of the electron density for the T75G (red) and the wild-type (black) channel is shown on the right.

using the modular approach. We observed that the rate of inactivation in the KcsA G79ester channel was very similar to that of the wild-type channel (Figure 6A and Table 1), as previously reported (Matulef et al., 2013). Measurements of recovery from inactivation indicated that the recovery also took place with a time course that was very similar to that of the wild-type control (Figure 6C and Table 1). These results show that the ion occupancy at the S1 site in the selectivity filter does not play a critical role in inactivation or in recovery in the KcsA channel.

Ion Occupancy at the S4 Site Enhances Recovery from Inactivation

The hydroxyl group of Thr75 contributes to the S4 site (Figure 1B). To elucidate the role of this site, we used side-chain substitutions that remove the hydroxyl group. We initially tested the T75C substitution, as loss of ion binding at the S4 site in this mutant has been crystallographically demonstrated (Zhou and MacKinnon, 2004). We were unable to detect macroscopic currents for the T75C mutant and therefore, we investigated other amino acid substitutions that also remove the hydroxyl group. Of the substitutions tested, we were able to measure robust macroscopic currents for the T75G mutant. We found that the T75G KcsA channel inactivates with a rate that was slightly (~2-fold) slower than that of the wild-type channel, while recovery was significantly impaired (~10-fold slower than the wild-type; Figures 7A and 7B; Table 1). We determined the structure of the T75G mutant to confirm that the Gly substitution does indeed affect the S4 site (Table 2). The electron density corresponding to the selectivity filter is shown in Figure 7C and shows the loss of the S4 site. A superposition of the selectivity filter of the T75G and the wild-type channel indicates that there are no structural changes in the selectivity filter other than the missing S4 site (Figure 7D). We observe some electron density at a lower site that we refer to as the S4′ site, and the 1D plot also shows a slight reduction in the ion occupancy at the S2 site, similarly to the KcsA T75C mutant (Figure 7E) (Zhou and MacKinnon, 2004). The major effects of the T75G substitution, i.e., loss of the S4 site and the reduction in the rate of recovery from inactivation, indicate that ion occupancy at the S4 site is important for recovery from inactivation.

Surprisingly, some crystals of the T75G mutant were found to have the selectivity filter in a non-conductive conformation that was similar to the constricted state (Figure S2). Our results with the G77dA substitution clearly demonstrate that the constricted state does not correspond to the C-type inactivated state (Devaraneni et al., 2013; Figures 4C and 4D), and therefore the physiological significance of this non-conductive conformation of the T75G mutant is presently not obvious.

Table 1. Inactivation Parameters

		Effect on Ion Occupancy	$\tau_{inactivation}$ (ms)	I_f/I_o	$\tau_{recovery}$ (s)
Wild-type	recombinant		1,820 ± 641 (16)	0.06 ± 0.04 (16)	3.8 ± 0.8
Control[a]	recombinant		2,803 ± 729 (9)	0.17 ± 0.10 (9)	2.5 ± 0.4
G79ester	semisynthetic	S1 ↓	3,636 ± 1,786 (9)	0.19 ± 0.07 (9)	3.0 ± 0.8
Y78ester[b]	recombinant	S2 ↓	NA	0.64 ± 0.09 (4)	NA
G77ester	semisynthetic	S2 ↓	NA	0.80 ± 0.15 (6)	NA
V76ester	semisynthetic	S3 ↓	5,821 ± 1,971 (12)	0.26 ± 0.12 (12)	81.3 ± 14.8
T75G	recombinant	S4 ↓	6,512 ± 2,663 (11)	0.29 ± 0.14 (11)	30.3 ± 4.0
G77dA	semisynthetic	–	2,850 ± 1,760 (6)	0.23 ± 0.10 (6)	3.2 ± 0.7
V76ester + G77dA	semisynthetic	S3 ↓	2,414 ± 526 (12)	0.19 ± 0.05 (12)	36.7 ± 1.9

Numbers represent mean ± SD. I_f/I_o is fraction of the current remaining at the end of the inactivation pulse divided by the peak current. The number of experiments are shown in parentheses. Standard deviations reported for $\tau_{recovery}$ were determined from the fits as described in Experimental Procedures.

[a]Control KcsA channel contains the S69A, V70C, and Y82C substitutions that were required for semisynthesis and are present in the semisynthetic channels.

[b]Recombinantly expressed using the nonsense suppression method (Matulef et al., 2013).

DISCUSSION

In this study we evaluate how the ion binding sites in the K^+ selectivity filter participate in C-type inactivation and in recovery from inactivation. We use amide-to-ester substitutions in the protein backbone of the selectivity filter to alter ion occupancy at the S1–S3 sites and use a T75G substitution to alter ion occupancy at the S4 site. We find that ion occupancy at the lower sites, S3 and S4, is required for recovery from inactivation, while ion occupancy at the S2 site is required for entry into the inactivated state (Figure 8A). Additionally we find that ion occupancy at the S1 site does not influence either inactivation or recovery. Our studies therefore reveal surprisingly distinct roles for the ion binding sites in the inactivation process.

The amide bonds in the selectivity filter form H bonds with the surrounding residues, and the amide-to-ester substitution results in the deletion of this H bond (Zhou et al., 2001). The functional effects of the ester substitutions on inactivation could potentially also arise due to the disruption of the H bond. However, the crystal structures for the 1′, 3′, and 4′ ester substitutions, which affect ion occupancies at the S1, S2, and S3 sites, respectively, show that these ester substitutions do not cause any appreciable changes in the structure of the selectivity filter or the surrounding residues. Furthermore, the 2′ and 3′ ester substitutions have similar effects on ion occupancy and inactivation, even though they disrupt different H bonds (Figure S1). Based on these observations, we can rule out disruption of the H bond as the major cause of the functional effects of the ester substitutions on the inactivation process. The ester bond also shows a lower rotational barrier compared with an amide bond. However, the ester linkage has a strong preference for the *trans* conformation, and the energy barrier for rotation of the ester bond is 10–15 kcal/mol (compared with 18–21 kcal/mol for an amide bond) (Choudhary and Raines, 2011). The barrier for rotation is sufficiently high that the ester substitution is not expected to cause an increase in dynamics of the peptide backbone. In support, we observe in the crystal structures that the ester linkages are ordered similarly to the neighboring amide bonds. We can therefore conclude that the functional effects of the ester substitutions on inactivation are predominantly due to the changes in ion occupancy at the selectivity filter sites.

The 2′, 3′, and 4′ carbonyl oxygens, which are affected by the Y78ester, G77ester, and V76ester substitutions, respectively, are involved in coordinating ions at two sites (Figure 1B). However, our structural studies show that these ester substitutions specifically decrease ion occupancy at only one site. The Y78ester and G77ester decrease ion occupancy at the S2 site, whereas the V76ester decreases ion occupancy specifically at the S3 site. We do not know the chemical reason for this specificity of the ester substitutions, but this fortuitous effect allowed us to investigate the role of the individual ion binding sites.

Our findings that ion occupancy at the S3 and the S4 sites is important for recovery from inactivation are consistent with the studies on the Shaker K^+ channel reported by Ray and Deutsch (2006), which concluded that recovery from inactivation is

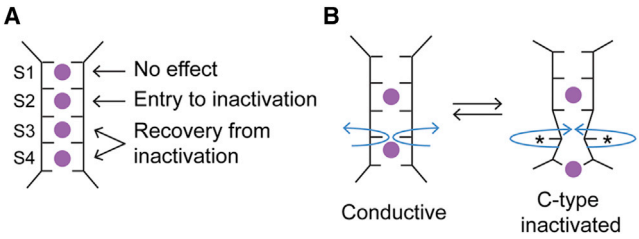

Figure 8. A Working Model for C-type Inactivation

(A) Summary of the effects of ion occupancy at the selectivity filter sites on inactivation and recovery.

(B) Schematic diagram of the selectivity filter in the conductive and inactivated states. The conformational change at the selectivity filter leading to C-type inactivation is proposed to be a rotation of the 4′ carbonyl oxygen that results in a disruption of the S3 and S4 sites. The inactivated state contains an ion bound at the S2 site. Recovery from inactivation involves a rotation of the 4′ carbonyl oxygen back into the conduction pathway to regenerate the S3 and the S4 sites. K^+ ions are represented as purple spheres. The 4′ carbonyl oxygen is indicated by an asterisk and the direction of movement by blue arrows.

Table 2. Crystallographic Data Collection and Model Refinement Statistics

	V76ester	V76ester + G77dA	G77ester
PDB ID	5EC1	5EC2	5EBW
Space group	I4	I4	I4
Cell dimensions			
a, *b*, *c* (Å)	155.6, 155.6, 75.64	154.8, 154.87, 75.703	156.91, 156.91, 75.837
α, β, γ (°)	90, 90, 90	90, 90, 90	90, 90, 90
Detector	ALS RDI_8M CMOS	ALS RDI_8M CMOS	ALS RDI_8M CMOS
Resolution (Å)	2.9	2.5	2.3
$CC_{1/2}$	0.998 (0.746)	0.999 (0.841)	0.998 (0.785)
$I/\sigma I$	15.5 (2.0)	15.6 (2.4)	13.1 (2.2)
Completeness	100.0 (100.0)	99.9 (100.0)	100 (100)
Multiplicity	14.7 (13.9)	7.4 (7.4)	7.5 (7.4)
No. of total reflections	293,467	231,082	306,427
No. of unique reflections	20,012	31,160	41,049
R_{work}/R_{free}[a]	24.4/26.8	23.0/25.9	22.2/24.9
Rmsd of bond lengths (Å)	0.004	0.003	0.004
Rmsd of bond angles (°)	0.67	0.69	0.81
Ramachandran plot[b] (%)			
Favored	96	97	97
Allowed	4	3	3
Outlier	0	0	0

	T75G Conductive	T75G Constricted
PDB ID	5EBL	5EBM
Space group	I4	I4
Cell dimensions		
a, *b*, *c* (Å)	155.41, 155.41, 76.27	155.72, 155.72, 75.556
α, β, γ (°)	90, 90, 90	90, 90, 90
Detector	ALS RDI_8M CMOS	ALS RDI_8M CMOS
Resolution (Å)	2.4	2.6
$CC_{1/2}$	0.998 (0.708)	0.999 (0.781)
$I/\sigma I$	14.6 (2.0)	17.4 (2.1)
Completeness	100.0 (100.0)	100.0 (100.0)
Multiplicity	7.2 (7.1)	7.1 (7.2)
No. of total reflections	256,726	199,097
No. of unique reflections	35,730	27,981
R_{work}/R_{free}[a]	20.5/24.2	21.6/25.1
Rmsd of bond lengths (Å)	0.003	0.005
Rmsd of bond angles (°)	0.80	0.73
Ramachandran plot[b] (%)		
Favored	97	97
Allowed	3	3
Outlier	0	0

Numbers in parentheses are statistics for the last resolution shell. Rmsd, root-mean-square deviation.

[a] $R = \sum|F_o - F_c|/\sum F_o$. 10% of the reflections that were excluded from the refinement were used in the R_{free} calculation.

[b] Performed in MolProbity.

dependent on ion binding to a selectivity filter site toward the intracellular side. Our findings are not in accord with the constricted- or the dilated-state models that have been put forth to describe the C-type inactivated state. The constricted model for the inactivated state was based on crystal structures of the KcsA channel trapped with the cytoplasmic gate open or in the presence of low concentrations of K^+ (Berneche and Roux, 2005; Cuello et al., 2010b; Yellen, 2001; Zhou et al., 2001). We confirmed our previous findings that the G77dA substitution, which blocks the constricted state, does not alter the rate and extent of inactivation or the rate of recovery (Devaraneni et al., 2013). This result demonstrates that the constricted state of the selectivity filter does not correspond to the physiologically relevant inactivated state. Furthermore, the constricted-state model predicts that inactivation proceeds through the loss of ion occupancy at the S2 site, while we observe that loss of ion occupancy at the S2 site (which we find with either the 2′ or the 3′ ester substitutions) actually impairs inactivation (Berneche and Roux, 2005; Cuello et al., 2010b). The dilation model, which is based on studies of eukaryotic K_v channels, proposes that C-type inactivation involves a widening of the S1 site, thereby rendering the channel non-conductive (Hoshi and Armstrong, 2013). We observe that a reduction in ion occupancy at the S1 site does not influence either inactivation or recovery from the inactivated state. Therefore, our results also do not support the dilated model for the C-type inactivated state. Our conclusions are based on studies of the KcsA channel, and it is possible that differences exist in the mechanism of inactivation in KcsA and other K^+ channels.

Our results provide clues about the ion binding sites that are distorted on inactivation, and suggest a working model for the structural changes that take place during inactivation (Figure 8B). For the S1 site, the lack of an effect on inactivation from a decrease in ion occupancy suggests that inactivation does not involve any changes at this site. The requirement of ion occupancy at the S2 site for channels to inactivate suggests that the inactivated state must contain an intact S2 site. For the S3 and S4 sites, we observe that ion occupancy is required for recovery from inactivation, which suggests that the inactivated state involves a distortion of S3 and S4 sites. This distortion could be a simple structural change such as a rotation of the 4′ amide bond that moves the carbonyl oxygen away from the ion conduction pathway. Such a rotation of the 4′ carbonyl oxygen will render the S3 and S4 sites unable to coordinate a K^+ ion and will create a barrier to the movement of ions through the filter. Recovery from inactivation would then involve the rotation of the 4′ carbonyl oxygen back into the ion conduction pathway to

reform the S3 and S4 sites, a process that is stabilized by ion binding to these sites.

Our model is based on the changes to the inactivation process that are caused by altering the ion occupancy in the conductive state of the selectivity filter. In our crystal structures, the cytoplasmic activation gate is closed while inactivation requires an open activation gate. This difference in the state of the activation gate does not affect our conclusions, as the ion occupancy of the selectivity filter (in the conductive state) is not expected to change on opening of the activation gate. This expectation is based on structural studies of the K_vAP and $K_v1.2$ channels (Jiang et al., 2003; Long et al., 2007), which were crystallized in the open-conductive state and show ion occupancies in the selectivity filter that are similar to the KcsA channel in the closed-conductive state.

C-type inactivation is a complex process that involves structural changes beyond the ion binding sites. There is a large body of evidence indicating that the structural changes on C-type inactivation involve amino acid side chains surrounding the selectivity filter and the extracellular vestibule (Cordero-Morales et al., 2006b, 2007, 2011; Larsson and Elinder, 2000; Liu et al., 1996; Loots and Isacoff, 1998; Pless et al., 2013; Raghuraman et al., 2014). Our results shed light on the role of selectivity filter sites during the inactivation process. Further studies will be necessary to determine how the changes in the selectivity filter sites during inactivation are propagated through the amino acid side chains surrounding the selectivity filter to the extracellular vestibule. Also presently unknown is the mechanism by which C-type inactivation is triggered by the opening of the activation gate.

This study highlights the utility of unnatural mutagenesis approaches for probing ion channel mechanisms. Conformational changes at the ion binding sites in the selectivity filter have been proposed to be important in the function of the BK channel, 2-pore K^+ channels, and also for channels outside the K^+ channel family such as TRP and CNG channels (Contreras et al., 2008; Flynn and Zagotta, 2001; Piechotta et al., 2011; Piskorowski and Aldrich, 2006; Thompson and Begenisich, 2012; Toth and Csanady, 2012). We anticipate that the amide-to-ester backbone mutagenesis strategy used in this study will be useful to elucidate the functional roles of the ion binding sites in these channels.

EXPERIMENTAL PROCEDURES

The G79ester, G77ester, V76ester, and V76ester + G77dA ester mutants of the KcsA channel were generated using the modular semisynthetic approach (Komarov et al., 2009). In the modular approach, the KcsA polypeptide is assembled from the three component peptides, a synthetic pore peptide corresponding to the selectivity filter and two recombinant fragments corresponding to the rest of the KcsA channel subunit. The peptides were linked together by two sequential NCL reactions followed by in vitro folding to the native state. To generate the ester mutants of the KcsA channel, we introduced the desired ester linkage during the synthesis of the pore peptide. The modular semisynthetic approach yields the full-length protein. Various steps of the modular semisynthesis were optimized as described in the Supplemental Experimental Procedures to improve the yields of the ester mutants. The KcsA G77ester channel used for structure determination was assembled using the two-part semisynthesis as previously described (Matulef et al., 2013). The wild-type and the T75G KcsA channels were expressed as previously described (Doyle et al., 1998). The semisynthetic and the recombinant KcsA channels were purified by immobilized metal-affinity chromatography followed by size-exclusion chromatography.

For functional studies, the purified KcsA channel mutants were reconstituted into lipid vesicles and channel activity was assayed by liposome patch clamping. Macroscopic currents for inactivation measurements were elicited by a pH jump from 8.0 to 3.0 on the cytoplasmic side. The time constants for inactivation were determined by single exponential fits. Recovery from inactivation was determined using a two-pulse protocol, with two activating steps to pH 3.0 separated by a variable recovery time at pH 8.0. The fractional recovery was determined by the ratio of the peak current in the second pulse to that of the first pulse. The recovery time constant ($\tau_{recovery}$) was determined by a fit to the equation $F = 1 - e^{-\left(\frac{t}{\tau_{recovery}}\right)}$, where F is the fractional recovery and t is the time interval at pH 8.0.

For crystallization of the KcsA channel mutants, the purification tags present and the C-terminal 35 amino acids (if present) were removed by proteolysis. The truncated KcsA channels were crystallized as a complex with an antibody Fab fragment from KcsA-IgG (Zhou et al., 2001). Structures were solved by molecular replacement using the wild-type KcsA channel structure (PDB: 1K4C) with the selectivity filter residues 75–79 omitted as the search model. The structures were modeled in Coot (Emsley and Cowtan, 2004) and refined using PHENIX (Adams et al., 2010). Model geometry was assessed using MolProbity (Chen et al., 2010). F_o-F_c maps shown were calculated with KcsA residues 75–79, K^+ ions and lipid omitted, and are depicted along the central axis of the selectivity filter. One-dimensional plots of electron density were calculated as previously described (Morais-Cabral et al., 2001; Zhou and MacKinnon, 2003).

Detailed methods are provided in Supplemental Experimental Procedures.

ACCESSION NUMBERS

Coordinates and structure factors have been deposited in the PDB under the accession codes PDB: 5EC1, 5EC2, 5EBW, 5EBL, and 5EBM for KcsA V76ester, KcsA V76ester+G77dA, KcsA G77ester, KcsA T75G conductive, and KcsA T75G constricted, respectively.

SUPPLEMENTAL INFORMATION

Supplemental Information includes Supplemental Experimental Procedures and two figures and can be found with this article online at http://dx.doi.org/10.1016/j.str.2016.02.021.

AUTHOR CONTRIBUTIONS

K.M. and F.I.V. conceived the project and wrote the paper. A.W.A. and F.I.V. assembled the semisynthetic channels. K.M. performed the electrophysiological characterization, crystallization, and structure determination. J.C.N. carried out the X-ray data collection.

ACKNOWLEDGMENTS

We thank Dr. R. MacKinnon for providing the Fab-expressing hybridoma cells, Daniel Cawley for monoclonal antibody production, and Dr. Michael Chapman and members of the Chapman group for answering our queries on X-ray crystallography. Part of this research was performed at the Advanced Light Source, which is supported by the Director, Office of Science, Office of Basic Energy Sciences, Materials Sciences Division, US Department of Energy, under contract no. DE-AC03-76SF00098, at Lawrence Berkeley National Laboratory. This research was supported by a grant from the NIH (GM087546) to F.I.V.

Received: December 29, 2015
Revised: February 8, 2016
Accepted: February 16, 2016
Published: April 14, 2016

REFERENCES

Adams, P.D., Afonine, P.V., Bunkoczi, G., Chen, V.B., Davis, I.W., Echols, N., Headd, J.J., Hung, L.W., Kapral, G.J., Grosse-Kunstleve, R.W., et al. (2010).

PHENIX: a comprehensive Python-based system for macromolecular structure solution. Acta Crystallogr. D Biol. Crystallogr. *66*, 213–221.

Ader, C., Schneider, R., Hornig, S., Velisetty, P., Vardanyan, V., Giller, K., Ohmert, I., Becker, S., Pongs, O., and Baldus, M. (2009). Coupling of activation and inactivation gate in a K^+-channel: potassium and ligand sensitivity. EMBO J. *28*, 2825–2834.

Armstrong, C.M., and Hoshi, T. (2014). K(+) channel gating: C-type inactivation is enhanced by calcium or lanthanum outside. J. Gen. Physiol. *144*, 221–230.

Berneche, S., and Roux, B. (2005). A gate in the selectivity filter of potassium channels. Structure *13*, 591–600.

Bhate, M.P., and McDermott, A.E. (2012). Protonation state of E71 in KcsA and its role for channel collapse and inactivation. Proc. Natl. Acad. Sci. USA *109*, 15265–15270.

Chakrapani, S., Cordero-Morales, J.F., and Perozo, E. (2007). A quantitative description of KcsA gating I: macroscopic currents. J. Gen. Physiol. *130*, 465–478.

Chen, V.B., Arendall, W.B., 3rd, Headd, J.J., Keedy, D.A., Immormino, R.M., Kapral, G.J., Murray, L.W., Richardson, J.S., and Richardson, D.C. (2010). MolProbity: all-atom structure validation for macromolecular crystallography. Acta Crystallogr. D Biol. Crystallogr. *66*, 12–21.

Choudhary, A., and Raines, R.T. (2011). An evaluation of peptide-bond isosteres. Chembiochem *12*, 1801–1807.

Contreras, J.E., Srikumar, D., and Holmgren, M. (2008). Gating at the selectivity filter in cyclic nucleotide-gated channels. Proc. Natl. Acad. Sci. USA *105*, 3310–3314.

Cordero-Morales, J.F., Cuello, L.G., and Perozo, E. (2006a). Voltage-dependent gating at the KcsA selectivity filter. Nat. Struct. Mol. Biol. *13*, 319–322.

Cordero-Morales, J.F., Cuello, L.G., Zhao, Y., Jogini, V., Cortes, D.M., Roux, B., and Perozo, E. (2006b). Molecular determinants of gating at the potassium-channel selectivity filter. Nat. Struct. Mol. Biol. *13*, 311–318.

Cordero-Morales, J.F., Jogini, V., Lewis, A., Vasquez, V., Cortes, D.M., Roux, B., and Perozo, E. (2007). Molecular driving forces determining potassium channel slow inactivation. Nat. Struct. Mol. Biol. *14*, 1062–1069.

Cordero-Morales, J.F., Jogini, V., Chakrapani, S., and Perozo, E. (2011). A multipoint hydrogen-bond network underlying KcsA C-type inactivation. Biophys. J. *100*, 2387–2393.

Cuello, L.G., Romero, J.G., Cortes, D.M., and Perozo, E. (1998). pH-dependent gating in the Streptomyces lividans K^+ channel. Biochemistry *37*, 3229–3236.

Cuello, L.G., Jogini, V., Cortes, D.M., Pan, A.C., Gagnon, D.G., Dalmas, O., Cordero-Morales, J.F., Chakrapani, S., Roux, B., and Perozo, E. (2010a). Structural basis for the coupling between activation and inactivation gates in K(+) channels. Nature *466*, 272–275.

Cuello, L.G., Jogini, V., Cortes, D.M., and Perozo, E. (2010b). Structural mechanism of C-type inactivation in K(+) channels. Nature *466*, 203–208.

Dawson, P.E., Muir, T.W., Clark-Lewis, I., and Kent, S.B. (1994). Synthesis of proteins by native chemical ligation. Science *266*, 776–779.

Devaraneni, P.K., Komarov, A.G., Costantino, C.A., Devereaux, J.J., Matulef, K., and Valiyaveetil, F.I. (2013). Semisynthetic K^+ channels show that the constricted conformation of the selectivity filter is not the C-type inactivated state. Proc. Natl. Acad. Sci. USA *110*, 15698–15703.

Doyle, D.A., Morais Cabral, J., Pfuetzner, R.A., Kuo, A., Gulbis, J.M., Cohen, S.L., Chait, B.T., and MacKinnon, R. (1998). The structure of the potassium channel: molecular basis of K^+ conduction and selectivity. Science *280*, 69–77.

Emsley, P., and Cowtan, K. (2004). Coot: model-building tools for molecular graphics. Acta Crystallogr. D Biol. Crystallogr. *60*, 2126–2132.

Flynn, G.E., and Zagotta, W.N. (2001). Conformational changes in S6 coupled to the opening of cyclic nucleotide-gated channels. Neuron *30*, 689–698.

Gao, L., Mi, X., Paajanen, V., Wang, K., and Fan, Z. (2005). Activation-coupled inactivation in the bacterial potassium channel KcsA. Proc. Natl. Acad. Sci. USA *102*, 17630–17635.

Hille, B. (2001). Ion Channels of Excitable Membranes (Sinauer).

Hoshi, T., and Armstrong, C.M. (2013). C-type inactivation of voltage-gated K+ channels: pore constriction or dilation? J. Gen. Physiol. *141*, 151–160.

Hoshi, T., Zagotta, W.N., and Aldrich, R.W. (1991). Two types of inactivation in Shaker K^+ channels: effects of alterations in the carboxy-terminal region. Neuron *7*, 547–556.

Imai, S., Osawa, M., Takeuchi, K., and Shimada, I. (2010). Structural basis underlying the dual gate properties of KcsA. Proc. Natl. Acad. Sci. USA *107*, 6216–6221.

Jiang, Y., Lee, A., Chen, J., Cadene, M., Chait, B.T., and MacKinnon, R. (2002). The open pore conformation of potassium channels. Nature *417*, 523–526.

Jiang, Y., Lee, A., Chen, J., Ruta, V., Cadene, M., Chait, B.T., and MacKinnon, R. (2003). X-ray structure of a voltage-dependent K^+ channel. Nature *423*, 33–41.

Kent, S.B. (1988). Chemical synthesis of peptides and proteins. Annu. Rev. Biochem. *57*, 957–989.

Komarov, A.G., Linn, K.M., Devereaux, J.J., and Valiyaveetil, F.I. (2009). Modular strategy for the semisynthesis of a K^+ channel: investigating interactions of the pore helix. ACS Chem. Biol. *4*, 1029–1038.

Kurata, H.T., and Fedida, D. (2006). A structural interpretation of voltage-gated potassium channel inactivation. Prog. Biophys. Mol. Biol. *92*, 185–208.

Larsson, H.P., and Elinder, F. (2000). A conserved glutamate is important for slow inactivation in K^+ channels. Neuron *27*, 573–583.

Liu, Y., Jurman, M.E., and Yellen, G. (1996). Dynamic rearrangement of the outer mouth of a K^+ channel during gating. Neuron *16*, 859–867.

Liu, Y., Holmgren, M., Jurman, M.E., and Yellen, G. (1997). Gated access to the pore of a voltage-dependent K^+ channel. Neuron *19*, 175–184.

Long, S.B., Tao, X., Campbell, E.B., and MacKinnon, R. (2007). Atomic structure of a voltage-dependent K^+ channel in a lipid membrane-like environment. Nature *450*, 376–382.

Loots, E., and Isacoff, E.Y. (1998). Protein rearrangements underlying slow inactivation of the Shaker K^+ channel. J. Gen. Physiol. *112*, 377–389.

MacKinnon, R. (2004). Nobel Lecture. Potassium channels and the atomic basis of selective ion conduction. Biosci. Rep. *24*, 75–100.

MacKinnon, R., Cohen, S.L., Kuo, A., Lee, A., and Chait, B.T. (1998). Structural conservation in prokaryotic and eukaryotic potassium channels. Science *280*, 106–109.

Matulef, K., Komarov, A.G., Costantino, C.A., and Valiyaveetil, F.I. (2013). Using protein backbone mutagenesis to dissect the link between ion occupancy and C-type inactivation in K^+ channels. Proc. Natl. Acad. Sci. USA *110*, 17886–17891.

McCoy, J.G., and Nimigean, C.M. (2012). Structural correlates of selectivity and inactivation in potassium channels. Biochim. Biophys. Acta *1818*, 272–285.

Morais-Cabral, J.H., Zhou, Y., and MacKinnon, R. (2001). Energetic optimization of ion conduction rate by the K^+ selectivity filter. Nature *414*, 37–42.

Muir, T.W. (2003). Semisynthesis of proteins by expressed protein ligation. Annu. Rev. Biochem. *72*, 249–289.

Panyi, G., and Deutsch, C. (2006). Cross talk between activation and slow inactivation gates of Shaker potassium channels. J. Gen. Physiol. *128*, 547–559.

Perozo, E., Cortes, D.M., and Cuello, L.G. (1999). Structural rearrangements underlying K^+-channel activation gating. Science *285*, 73–78.

Piechotta, P.L., Rapedius, M., Stansfeld, P.J., Bollepalli, M.K., Ehrlich, G., Andres-Enguix, I., Fritzenschaft, H., Decher, N., Sansom, M.S., Tucker, S.J., et al. (2011). The pore structure and gating mechanism of K2P channels. EMBO J. *30*, 3607–3619.

Piskorowski, R.A., and Aldrich, R.W. (2006). Relationship between pore occupancy and gating in BK potassium channels. J. Gen. Physiol. *127*, 557–576.

Pless, S.A., Galpin, J.D., Niciforovic, A.P., Kurata, H.T., and Ahern, C.A. (2013). Hydrogen bonds as molecular timers for slow inactivation in voltage-gated potassium channels. Elife *2*, e01289.

Powers, E.T., Deechongkit, S., and Kelly, J.W. (2005). Backbone-backbone h-bonds make context-dependent contributions to protein folding kinetics

and thermodynamics: lessons from amide-to-ester mutations. Adv. Protein Chem. *72*, 39–78.

Raghuraman, H., Islam, S.M., Mukherjee, S., Roux, B., and Perozo, E. (2014). Dynamics transitions at the outer vestibule of the KcsA potassium channel during gating. Proc. Natl. Acad. Sci. USA *111*, 1831–1836.

Ray, E.C., and Deutsch, C. (2006). A trapped intracellular cation modulates K^+ channel recovery from slow inactivation. J. Gen. Physiol. *128*, 203–217.

Tao, X., Avalos, J.L., Chen, J., and MacKinnon, R. (2009). Crystal structure of the eukaryotic strong inward-rectifier K^+ channel Kir2.2 at 3.1 A resolution. Science *326*, 1668–1674.

Thompson, J., and Begenisich, T. (2012). Selectivity filter gating in large-conductance Ca(2+)-activated K(+) channels. J. Gen. Physiol. *139*, 235–244.

Toth, B., and Csanady, L. (2012). Pore collapse underlies irreversible inactivation of TRPM2 cation channel currents. Proc. Natl. Acad. Sci. USA *109*, 13440–13445.

Twibanire, J.D., and Grindley, T.B. (2011). Efficient and controllably selective preparation of esters using uronium-based coupling agents. Org. Lett. *13*, 2988–2991.

Valiyaveetil, F.I., Sekedat, M., Muir, T.W., and MacKinnon, R. (2004). Semisynthesis of a functional K^+ channel. Angew. Chem. Int. Ed. Engl. *43*, 2504–2507.

Valiyaveetil, F.I., Leonetti, M., Muir, T.W., and Mackinnon, R. (2006a). Ion selectivity in a semisynthetic K^+ channel locked in the conductive conformation. Science *314*, 1004–1007.

Valiyaveetil, F.I., Sekedat, M., MacKinnon, R., and Muir, T.W. (2006b). Structural and functional consequences of an amide-to-ester substitution in the selectivity filter of a potassium channel. J. Am. Chem. Soc. *128*, 11591–11599.

Yellen, G. (2001). Keeping K^+ completely comfortable. Nat. Struct. Biol. *8*, 1011–1013.

Zhou, Y., and MacKinnon, R. (2003). The occupancy of ions in the K^+ selectivity filter: charge balance and coupling of ion binding to a protein conformational change underlie high conduction rates. J. Mol. Biol. *333*, 965–975.

Zhou, M., and MacKinnon, R. (2004). A mutant KcsA K(+) channel with altered conduction properties and selectivity filter ion distribution. J. Mol. Biol. *338*, 839–846.

Zhou, Y., Morais-Cabral, J.H., Kaufman, A., and MacKinnon, R. (2001). Chemistry of ion coordination and hydration revealed by a K^+ channel-Fab complex at 2.0 Å resolution. Nature *414*, 43–48.